APSIPA Transactions on Signal and Information Processing, 2023, 12, e1

Original Paper

Energy Efficient Cloud Radio Access Network with Antenna Arrays

Chi-Chen Wang[1,2], Yan-Yin He[1,2] and Shang-Ho (Lawrence) Tsai[1,2*]

[1] *Institute of Electrical and Control Engineering, National Yang Ming Chiao Tung University, Hsinchu 300, Taiwan*

[2] *National Chiao Tung University, Hsinchu 300, Taiwan*

ABSTRACT

This work aims to improve the energy efficiency of cloud radio access network (C-RAN). Power consumption is an important issue in deploying dense small cell networks such as C-RAN, especially for millimeter wave (mmWave) band where systems generally consume large power due to having massive phase shifters. To address this issue, we propose three different solutions to design the C-RAN beamforming to minimize power consumption under fixed user target rates. The first and second solutions are respectively based on the second-order cone programming (SOCP) and the semidefinite programming (SDP). Inspired by the results, we propose the third solution, which has a closed-form expression. The numerical results of these three solutions are extremely close. Since the first two solutions are obtained by standard optimization methods SOCP and SDP, which require high computational complexity, in most cases one can use the third solution to achieve comparable performance with significantly lower complexity. Based on the proposed beamforming solutions, the phase shifters of the array antennas can be selected and turned off to further significantly reduce the power consumption. Simulation results show that overall power consumption of C-RAN can be greatly decreased using the proposed schemes.

*Corresponding author: Shang-Ho (Lawrence) Tsai, shanghot@alumni.usc.edu

Received 03 June 2022; Revised 06 September 2022
ISSN 2048-7703; DOI 10.1561/116.00000036

1 Introduction

Cloud radio access network (C-RAN) has received extensive attention in 5G/B5G communications, because it provides high data rate transmission as well as better coverage by deploying dense small cells. In C-RAN, a large portion of hardware and computational complexity is relocated to baseband units (BBUs), and thus the traditional full-function base stations can be replaced by low-cost remote radio heads (RRHs), which handle data transmission and reception with user equipments (UEs) [15, 20, 23]. Energy efficiency is one of the important performance metrics in 5G communications. When the target rate is fixed, maximizing energy efficiency becomes minimizing power consumption. For dense deployments of C-RAN, power consumption is considerable and should be carefully controlled. Thus, research has been conducted in maximizing the energy efficiency for MIMO C-RAN [1, 4, 9, 21, 25, 26, 30, 31]. More specifically, the authors in [25] proposed precoders to maximize energy efficiency under both data-sharing and compression-based strategies. In [4, 21, 31], precoders were designed to optimize the total network power consumption. In [26], the authors designed a precoder to minimize the power of a wireless fronthaul network with considerations of channel uncertainty. In [30], a precoder was designed to make a trade-off between network capacity and power consumption. Additionally, to optimize the energy efficiency, two power allocation techniques in the NOMA-based two tiers C-RAN were revealed in [1] and a double deep Q network (DDQN) framework was investigated in [9].

The importance of minimizing power consumption for C-RAN becomes more pronounced in mmWave channels, where array antennas are generally adopted and this leads to high power consumption due to the large amount of phase shifters. Most works designed precoders to maximize the throughput for C-RAN in mmWave channels, see [16] and [10]. Several studies pointed out that certain advantages may be achieved for systems with antenna arrays by turning off phase shifters or replacing phase shifters with switches [5, 11, 14, 17–19]. To name a few, in [17], a novel phase shifter selection method was proposed to reduce power consumption as well as achieve higher spectral efficiency. The authors in [5] proposed a sub-connected architecture between RF chains and antennas, which can save power by reducing phase shifters. The studies in [11, 14, 18, 19] were proposed to cut down power consumption via switching off the phase shifters. The authors in [19] compared the pros and cons for several hybrid beamforming architectures including fully connected, subconnected, subconnected with phase shifter selection, and subconnected with reduced number of phase shifters. In [18], the authors suggested that combining usage of phase shifters and switches can attain more energy efficiency. The study in [11] proposed an SI-based hybrid precoding architecture that can achieve higher energy efficiency than traditional architectures.

As discussed above, millimeter wave communications demand high power consumption, and this issue becomes more pronounced in C-RAN due to the dense deployment of small cells. Hence it is of great desire to develop solutions to reduce the power consumption for C-RAN in mmWave channels. As mentioned in [5, 11, 14, 17–19] that the operation of phase shifters occupies a large percentage of the power consumption, they suggested turning off or replacing phase shifters by switches to decrease the power consumption. Although these works are not for C-RAN in mmWave channels and their objective functions are to maximize the achievable rate, they still motivate us to solve the power consumption issue for C-RAN in mmWave environments by changing the objective function to minimize the power, and properly selecting and turning off partial phase shifters.

In this work, we propose solutions to reduce the power consumption for C-RAN in mmWave channels by properly selecting and turning off partial phase shifters. More specifically, the objective function is set to minimize the power under fixed target rates for individual UEs. Although similar problems may have been studied, however, this work has several differences from existing literature. First, although the studies in [1, 4, 9, 21, 25, 26, 30, 31] applied the C-RAN architectures and provided the power consumption models, seeming to handle tasks similar to those in this work, their models however vary from that in this work. Thus the related parameters are also much different from ours. Additionally, in this work, we consider to turn off phase shifters of array antenna to minimize the power consumption, which is not the case in these studies. For the studies in [5, 11, 14, 17–19], they are not in the C-RAN architectures, and the objective problems are not minimizing power consumption. Moreover, the users' target rate constraints in this work are not considered in these studies.

We propose three different solutions for this problem, including two standard optimization methods and one closed-form solution. The first solution is obtained by treating the issue as a standard second-order cone programming (SOCP) problem and solving it numerically via convex optimization techniques. In the second solution, we use the well-known semidefinite relaxation (SDR) technique to rewrite the problem as a standard semidefinite programming (SDP) problem and then solve it numerically via convex optimization techniques. From the first and second solutions, we gain insight that in these two solutions, the multiuser interference is negligible, which inspires us to utilize this insight to develop the third solution. Moreover, since the two solutions are both done numerically, they demand high computational complexity, especially in this multi-cell network with array antennas. Inspired by these two solutions and going to overcome their complexity issues as well, we further propose the third solution that is a closed-form solution and can significantly reduce the computational time. Based on the solutions, algorithms

are proposed to properly select phase shifters and turn them off to reduce the power consumption.

Simulation results are provided to show the correctness and advantages of the proposed solutions. First, we find that although the three solutions are obtained through different methods, they all lead to similar numerical results, which validates the correctness of these results. Second, because all the solutions have similar numerical results, one may simply use Solution 3 that has the lowest computational complexity, where simulation results show that its computational complexity is less than 1/100 of those in both Solutions 1 and 2. Third, by using the proposed solutions and phase shifter selection algorithm, the power consumption can be significantly reduced, e.g., from 20 Watts to 5 Watts, in a setting with 64 transmit antennas, 3 UEs and 3 RRHs. Finally, since the phase shifters are turned off to reduce the power consumption, we are also interested in how this turning off changes the resulting beam patterns and whether or not this is practical in wireless environments. To see this, we conduct simulations using a ray tracing tool named Wireless InSite [28] and observe the resulting beam patterns when the phase shifters are turned off. The results show that the beam patterns from the RRHs still reasonably point to UEs when some of the phase shifters are turned off.

2 System Model, Problem Formulation, and Background Review

2.1 Proposed C-RAN Architecture

Consider a downlink C-RAN system in Figure 1. Assume that there are K UEs with a single antenna per UE, N RRHs with M_t antennas per RRH, and one BBU. Each UE links to the RRHs via the wireless network, and the RRHs link to the BBU via an error-free, highspeed, and low-latency fronthaul link, where each RRH is equipped with $N_{RF} = K$ RF chains. Each RF chain is connected to all transmit antennas through the phase shifters with variable gains [2]. Moreover, the BBU is assumed to have the full channel state information (CSI) of all UEs.

At the RRH side, each RRH transmits signals to the UEs synchronously. Let $\mathbf{s}_n$ be the data vector from the n-th RRH, i.e., $\mathbf{s}_n = [s_1\ s_2\ \cdots\ s_K]^T$, where s_k is the data for the k-th UE and its power is $\mathbb{E}\{s_k s_k^*\} = 1$, $\forall k = 1, \cdots, K$. The notation $[\mathbf{s}_n]_k$ is defined as the k-th element of vector $\mathbf{s}_n$ which represents the data for the k-th UE. Moreover, the data sent to the k-th UE from different RRHs is assumed to be the same, i.e., $[\mathbf{s}_n]_k = [\mathbf{s}_j]_k, \forall n \neq j$ where $n, j = 1, \cdots, N$. Let the channel vector from the n-th RRH to the k-th UE be $\mathbf{h}_{k,n}^H \in \mathbb{C}^{1\times M_t}$. In addition, let the analog precoder at the n-th RRH be $\mathbf{F}_n \in \mathbb{C}^{M_t \times N_{RF}}$ and its k-th column be $\mathbf{f}_{n,k}$, where $\mathbf{f}_{n,k}$ can therefore represent the analog precoder for the k-th UE at the n-th RRH. Then, the received

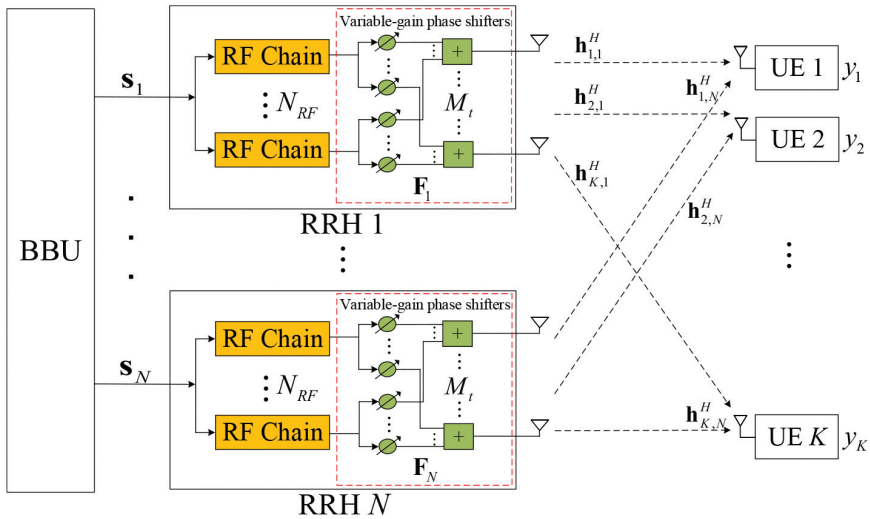

Figure 1: The proposed downlink C-RAN architecture.

signal y_k at the k-th UE can be expressed as

$$\begin{aligned} y_k &= \sum_{n=1}^{N} \mathbf{h}_{k,n}^H \mathbf{F}_n \mathbf{s}_n + w_k \\ &= \sum_{n=1}^{N} \mathbf{h}_{k,n}^H \sum_{l=1}^{K} \mathbf{f}_{n,l} [\mathbf{s}_n]_l + w_k \\ &= \underbrace{\sum_{n=1}^{N} \mathbf{h}_{k,n}^H \mathbf{f}_{n,k} [\mathbf{s}_n]_k}_{\text{desired signal}} + \underbrace{\sum_{n=1}^{N} \mathbf{h}_{k,n}^H \sum_{l \neq k}^{K} \mathbf{f}_{n,l} [\mathbf{s}_n]_l}_{\text{interference}} + w_k \\ &= \mathbf{h}_k^H \mathbf{f}_k s_k + \mathbf{h}_k^H \sum_{l \neq k}^{K} \mathbf{f}_l s_l + w_k, \end{aligned} \tag{1}$$

where the equivalent channel vector $\mathbf{h}_k^H$ for the k-th UE can be written as

$$\mathbf{h}_k^H = \begin{bmatrix} \mathbf{h}_{k,1}^H & \mathbf{h}_{k,2}^H & \cdots & \mathbf{h}_{k,N}^H \end{bmatrix}, \tag{2}$$

and the equivalent analog precoder $\mathbf{f}_k$ for the k-th UE from all RRHs can be expressed as

$$\mathbf{f}_k = \begin{bmatrix} \mathbf{f}_{1,k}^T & \mathbf{f}_{2,k}^T & \cdots & \mathbf{f}_{N,k}^T \end{bmatrix}^T. \tag{3}$$

Moreover, w_k is the noise for the k-th UE, which has i.i.d. complex Gaussian distribution with zero mean and variance $\sigma_{w_k}^2$.

From (1), the received signal-to-interference-plus-noise ratio (SINR) at the k-th UE can be expressed as

$$\mathrm{SINR}_k = \frac{\left|\mathbf{h}_k^H \mathbf{f}_k\right|^2}{\sum_{l \neq k}^{K} \left|\mathbf{h}_k^H \mathbf{f}_l\right|^2 + \sigma_{w_k}^2}, \tag{4}$$

and the achievable rate for the k-th UE is given by

$$R_k = \log_2(1 + \mathrm{SINR}_k). \tag{5}$$

2.2 Power consumption model

From the system model in Figure 1, the power consumption of the n-th RRH P_n^{RRH} can be expressed as

$$P_n^{RRH} = \frac{1}{\eta_n} \left\|\mathbf{F}_n\right\|_F^2 + \underbrace{N_{RF} P_{RF} + \sum_{j=1}^{N_{RF}} \sum_{i=1}^{M_t} \left\| \left[\mathbf{F}_n\right]_{i,j} \right\|_0 P_{PS}}_{\text{hardware power consumption}}, \tag{6}$$

where $\left\|\mathbf{F}_n\right\|_F^2 = P_{n,tx}$ is the transmission power of the n-th RRH. η_n is the drain efficiency of the power amplifier [4, 13, 21, 31]. Moreover, P_{RF} and P_{PS} are the power consumption of individual RF chains and phase shifters respectively, which are regarded as hardware power consumption. According to [5, 11, 17, 19], turning off phase shifters can thus reduce the hardware power consumption. $[\mathbf{F}_n]_{i,j}$ represents the analog precoder of the j-th RF chain to the i-th antenna at the n-th RRH. The l_0-norm of a vector is defined as the number of non-zero entries in the vector. Hence $\|[\mathbf{F}_n]_{i,j}\|_0 = 1$ means that the value of the corresponding element of the analog precoder is not zero. Additionally, it also indicates that the corresponding phase shifter is used. On the other hand, $\|[\mathbf{F}_n]_{i,j}\|_0 = 0$ means that the value of the corresponding element of the analog precoder is zero and the corresponding phase shifter is turned off. As a result, one can utilize this function to determine whether the phase shifter is turned on or off. From (6), the total power consumption from all RRHs can then be expressed as

$$P_{total} = \sum_{n=1}^{N} P_n^{RRH}. \tag{7}$$

2.3 Problem Formulation

The goal is to minimize the total power consumption under the constraints that the transmission power of each RRH can not exceed its power constraint

and all UEs should achieve their target rates. This problem is equivalent to maximizing the energy efficiency defined as $\frac{\sum_k R_k}{P_{total}}$, which has become an important performance metric in 5G communications. The design problem can be written as

$$\begin{aligned} \underset{\mathbf{F}_1,\cdots,\mathbf{F}_N}{\text{minimize}} \quad & \sum_{n=1}^{N} \Big(\frac{1}{\eta_n}\|\mathbf{F}_n\|_F^2 + N_{RF}P_{RF} + \sum_{j=1}^{N_{RF}}\sum_{i=1}^{M_t}\|[\mathbf{F}_n]_{i,j}\|_0 P_{PS}\Big), \\ \text{s.t.} \quad & \|\mathbf{F}_n\|_F^2 \le \mathcal{P}_n, \quad \log_2(1+\text{SINR}_k) \ge \mathcal{R}_k, \end{aligned} \tag{8}$$

where $\mathcal{P}_n$ is the transmission power constraint at the n-th RRH, and $\mathcal{R}_k$ is the given target rate of the k-th UE. Problem in (8) is a joint design problem of transmit beamforming and phase shifter selection. Referring to (8), neither the l_0-norm term of the objective function nor the target rate constraint is convex, which is difficult to be solved in general. The proposed solutions are introduced in the following section.

3 Proposed Solutions

To solve the problem in (8), we propose a two-step solution. In the first step, we propose three different precoder solutions to minimize the transmission power consumption, and then in the second step we propose a greedy method to determine which phase shifters should be turned off based on the proposed precoding solutions.

Let us stick on the first step to design precoder that minimizes the power consumption below. In the first step, we assume that all phase shifters are enabled to design the precoder, i.e., $\|[\mathbf{F}_n]_{i,j}\|_0 = 1, \forall i = 1, 2, \cdots, M_t$, $j = 1, 2, \cdots, N_{RF}$, and $n = 1, 2, \cdots, N$. Thus, we can treat the hardware power consumption as a constant and omit it temporarily in the objective function. Then, the problem in the first step becomes

$$\begin{aligned} \underset{\mathbf{F}_1,\cdots,\mathbf{F}_N}{\text{minimize}} \quad & \sum_{n=1}^{N} \|\mathbf{F}_n\|_F^2, \\ \text{s.t.} \quad & \|\mathbf{F}_n\|_F^2 \le \mathcal{P}_n, \quad \log_2(1+\text{SINR}_k) \ge \mathcal{R}_k. \end{aligned} \tag{9}$$

In the following subsections, we propose three solutions for the problem in (9). Two of the three solutions are obtained by first reformulating the problem into two different types of standard convex optimization problems, which are respectively the SOCP and SDP, and then solving them by the interior-point method. Next, we observe the results of these two solutions and propose the third solution that can be expressed in closed-form and thus can significantly reduce the computational complexity.

3.1 Proposed Solution 1: Second-order Cone Programming (SOCP)

In this subsection, we reformulate the problem into an SOCP [4, 27]. By using the matrix norm theorem, $\|\mathbf{F}_n\|_F^2 = \sum_{k=1}^{K} \|\mathbf{f}_{n,k}\|_2^2$, and the fact that designing $\{\mathbf{f}_k\}_{k=1}^K$ is equivalent to designing $\{\{\mathbf{f}_{n,k}\}_{n=1}^N\}_{k=1}^K$, the problem in (9) is equivalent to

$$\begin{aligned} \underset{\{\{\mathbf{f}_{n,k}\}_{n=1}^N\}_{k=1}^K}{\text{minimize}} \quad & \sum_{n=1}^{N}\sum_{k=1}^{K} \|\mathbf{f}_{n,k}\|_2^2, \\ \text{s.t.} \quad & \sum_{k=1}^{K} \|\mathbf{f}_{n,k}\|_2^2 \le \mathcal{P}_n, \quad |\mathbf{h}_k^H \mathbf{f}_k|^2 \ge \alpha_k \left(\sum_{l \ne k}^{K} |\mathbf{h}_k^H \mathbf{f}_l|^2 + \sigma_{w_k}^2 \right), \end{aligned} \tag{10}$$

where $\alpha_k = 2^{\mathcal{R}_k} - 1$. The problem in (10) is non-convex since the second constraint is non-convex. However, one can reformulate it using the following lemma.

Lemma 1. *The target rate constraint in (10) can be reformulated as*

$$\text{Re}(\boldsymbol{h}_k^H \boldsymbol{f}_k) \ge \sqrt{\alpha_k} \left\| [\boldsymbol{h}_k^H \boldsymbol{f}_1 \ \boldsymbol{h}_k^H \boldsymbol{f}_2 \ \cdots \ \boldsymbol{h}_k^H \boldsymbol{f}_{k-1} \boldsymbol{h}_k^H \boldsymbol{f}_{k+1} \ \cdots \ \boldsymbol{h}_k^H \boldsymbol{f}_K \ \sigma_{w_k}] \right\|_2. \tag{11}$$

Proof. See Appendix. □

Using Lemma 1, the problem in (10) is transformed into a convex SOCP problem and can be effectively solved by the interior-point method.

3.2 Proposed Solution 2: Semidefinite Programming (SDP)

Let us consider the same problem in (9). Assume that the per RRH power constraint of the problem in (9) does not exceed the upper bound. One can reformulate the objective function of the problem using the matrix norm theorem, i.e., $\sum_{n=1}^{N} \|\mathbf{F}_n\|_F^2 = \sum_{k=1}^{K} \|\mathbf{f}_k\|_2^2$, where $\mathbf{f}_k$ is defined in (3). Thus, the objective function in (9) can be expressed as

$$\underset{\mathbf{f}_1,\cdots,\mathbf{f}_K}{\text{minimize}} \ \sum_{k=1}^{K} \|\mathbf{f}_k\|_2^2. \tag{12}$$

Using the property that $\|\mathbf{a}\|_2^2 = Tr(\mathbf{a}\mathbf{a}^H)$ and from (9) and (12), one can rewrite the problem as an SDP problem as follows:

$$\begin{aligned} \underset{\mathbf{f}_1,\cdots,\mathbf{f}_K}{\text{minimize}} \quad & \sum_{k=1}^{K} Tr(\mathbf{f}_k \mathbf{f}_k^H), \\ \text{s.t.} \quad & \log_2 \left(1 + \frac{Tr(\mathbf{h}_k \mathbf{h}_k^H \mathbf{f}_k \mathbf{f}_k^H)}{\sum_{l \ne k}^{K} Tr(\mathbf{h}_k \mathbf{h}_k^H \mathbf{f}_l \mathbf{f}_l^H) + \sigma_{w_k}^2} \right) \ge \mathcal{R}_k. \end{aligned} \tag{13}$$

However, one still needs to handle the non-convex target rate constraint. Thus, we introduce new variables $\mathbf{Q}_k = \mathbf{f}_k\mathbf{f}_k^H$ and $\mathbf{H}_k = \mathbf{h}_k\mathbf{h}_k^H$ to the problem in (13). $\mathbf{Q}_k$ and $\mathbf{H}_k$ are both rank one symmetric positive semidefinite (PSD) matrices, and $Tr(\mathbf{Q}_k)$ represents the transmission power of all RRHs to the k-th UE. Consequently, the problem can be rewritten as follows:

$$\begin{aligned} \underset{\mathbf{Q}_1,\cdots,\mathbf{Q}_K}{\text{minimize}} \quad & \sum_{k=1}^{K} Tr(\mathbf{Q}_k), \\ \text{s.t.} \quad & Tr(\mathbf{H}_k\mathbf{Q}_k) - \alpha_k \sum_{l\neq k}^{K} Tr(\mathbf{H}_k\mathbf{Q}_l) \geq \alpha_k\sigma_{w_k}^2, \quad \mathbf{Q}_k \succeq 0, \end{aligned} \tag{14}$$

where $\alpha_k = 2^{\mathcal{R}_k} - 1$ and $\mathbf{Q}_k$ can be relaxed by a rank relaxation method, i.e., the well-known semidefinite relaxation (SDR) method [12, 29]. One can see that the target rate constraint and the objective function are all affine functions of $\mathbf{Q}_k$. Thus, the problem in (14) can be solved by the interior-point method.

After $\mathbf{Q}_k$ is solved, the solution of $\mathbf{f}_k$ can be obtained from $\mathbf{Q}_k$ by using singular value decomposition (SVD) procedure, i.e., $\mathbf{f}_k = \sqrt{\sigma_o(\mathbf{Q}_k)}\mathbf{u}_o(\mathbf{Q}_k)$, where $\sigma_o(\mathbf{Q}_k)$ and $\mathbf{u}_o(\mathbf{Q}_k)$ are the maximum singular value of $\mathbf{Q}_k$ and its corresponding left singular vector, respectively.

Although Solutions 1 and 2 perform well, they both use interior-point methods where iterations are needed. As a result, the computational complexity grows and they may not be suitable for applications with fixed complexity, e.g., integrated circuit (IC) designs. Therefore, in the following subsection, we propose another closed-form solution with low complexity to overcome this issue.

3.3 Proposed Solution 3: Low-Complexity Closed-form Solution

Following the problem in (14) and the same variable definitions, one can obtain $\mathbf{Q}_k = \sigma_o(\mathbf{Q}_k)\mathbf{u}_o(\mathbf{Q}_k)\mathbf{u}_o(\mathbf{Q}_k)^H$ and $\mathbf{H}_k = \sigma_o(\mathbf{H}_k)\mathbf{u}_o(\mathbf{H}_k)\mathbf{u}_o(\mathbf{H}_k)^H$, respectively. The objective function in (14) can be reformulated as

$$\underset{\mathbf{Q}_1,\cdots,\mathbf{Q}_K}{\text{minimize}} \sum_{k=1}^{K} Tr(\sigma_o(\mathbf{Q}_k)\mathbf{u}_o(\mathbf{Q}_k)\mathbf{u}_o(\mathbf{Q}_k)^H). \tag{15}$$

Using the fact that $Tr(\mathbf{u}_o(\mathbf{Q}_k)\mathbf{u}_o(\mathbf{Q}_k)^H) = 1$, (15) can be rewritten. Thus, the problem in (14) becomes

$$\begin{aligned} \underset{\mathbf{Q}_1,\cdots,\mathbf{Q}_K}{\text{minimize}} \quad & \sum_{k=1}^{K} \sigma_o(\mathbf{Q}_k), \\ \text{s.t.} \quad & Tr(\mathbf{H}_k\mathbf{Q}_k) - \alpha_k \sum_{l\neq k}^{K} Tr(\mathbf{H}_k\mathbf{Q}_l) \geq \alpha_k\sigma_{w_k}^2. \end{aligned} \tag{16}$$

From (16), an intuitive way to minimize $\sigma_o(\mathbf{Q}_k)$ is to eliminate the interference term of the constraint and make it become as follows: s.t. $Tr(\mathbf{H}_k\mathbf{Q}_k) \geq \alpha_k\sigma_{w_k}^2$. In fact, this is a reasonable solution because we learned from the previous two proposed solutions in Subsections 3.1 and 3.2 that the interference tends to decrease significantly as the number of antennas of individual RRHs increases. This result is shown in the following example.

3.3.1 Example 1: Multiuser interference in Proposed Solutions 1 and 2

In this example, we show that the multiuser interference is negligible compared to the received power applying Solutions 1 and 2. The parameters are as follows: the target rate of each UE is 3 bits/s/Hz, $N = 3$, and $K = 3$. The signal to interference ratios (SIRs) for the two solutions are shown in Figure 2. The horizontal axis is the number of antennas at each RRH and the vertical axis is the value of SIR. Observe that the interference power caused by the two solutions is small, which results in large value of SIR, and this is more pronounced as M_t increases.

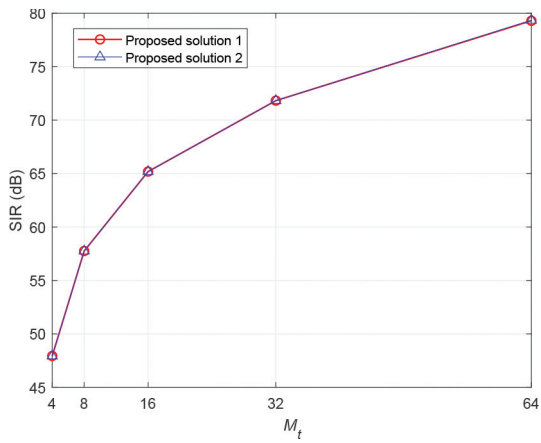

Figure 2: The desired signal power to interference power ratio under $K = 3$ and $N = 3$.

From Example 1, we know that the multiuser interference decreases as M_t increases. That is, the interference tends to be negligible for using the first two solutions as M_t increases. This inspires us to consider interference-free solutions. To proceed this, $\mathbf{u}_o(\mathbf{Q}_k)$ can be constructed via the null space of the interference channel, i.e., $Tr(\mathbf{H}_l\mathbf{Q}_k) = 0$, $\forall l \neq k$. Let the interference channel of the k-th UE be

$$\bar{\mathbf{H}}_k = \begin{bmatrix} \mathbf{h}_1 & \mathbf{h}_2 & \cdots & \mathbf{h}_{k-1} & \mathbf{h}_{k+1} & \cdots & \mathbf{h}_K \end{bmatrix}^H. \tag{17}$$

Denote $\mathbf{N}_k \in \mathbb{C}^{NM_t \times (NM_t-(K-1))}$ as the null space of $\bar{\mathbf{H}}_k \in \mathbb{C}^{(K-1)\times NM_t}$ whose column vectors are orthogonal bases. Let $\mathbf{u}_o(\mathbf{Q}_k)$ be the linear combination of the column vectors of $\mathbf{N}_k$. Hence $\mathbf{u}_o(\mathbf{Q}_k)$ is also in the null space of the interference channel, and one can construct it as

$$\mathbf{u}_o(\mathbf{Q}_k) = \mathbf{N}_k \mathbf{x}_k, \tag{18}$$

where $\mathbf{x}_k$ is the coefficient vector. Since the interference has been eliminated from the above process, the problem in (16) can be shown to be

$$\begin{aligned} \underset{\sigma_o(\mathbf{Q}_k),\ \mathbf{x}_k}{\text{minimize}} \quad & \sigma_o(\mathbf{Q}_k), \\ \text{s.t.} \quad & Tr(\sigma_o(\mathbf{H}_k)\mathbf{u}_o(\mathbf{H}_k)\mathbf{u}_o(\mathbf{H}_k)^H \sigma_o(\mathbf{Q}_k)\mathbf{N}_k\mathbf{x}_k(\mathbf{N}_k\mathbf{x}_k)^H) \geq \alpha_k \sigma_{w_k}^2. \end{aligned} \tag{19}$$

Please note that compared to the original problem in (16), the problem in (19) is no longer the original one because we have restricted the solution spanned by the null space of the interference channel, making the possible solutions in the subspace of the original solution space. The solution for (19) is provided in the following proposition.

Proposition 1. *The solution for the problem in (19) is given by*

$$\boldsymbol{x}_k = \boldsymbol{v}_o(\boldsymbol{G}_k), \tag{20}$$

where $\boldsymbol{G}_k = \boldsymbol{N}_k^H \boldsymbol{u}_o(\boldsymbol{H}_k)\boldsymbol{u}_o(\boldsymbol{H}_k)^H \boldsymbol{N}_k$ *and* $\mathbf{v}_o(\boldsymbol{G}_k)$ *is the eigenvector corresponding to the largest eigenvalue of* $\boldsymbol{G}_k$.

Proof. See Appendix. □

After obtaining the result in Proposition 1, one knows that

$$\mathbf{u}_o(\mathbf{Q}_k) = \mathbf{N}_k \mathbf{x}_k = \mathbf{N}_k \mathbf{v}_o(\mathbf{G}_k). \tag{21}$$

Now, referring to (19), one can obtain the minimum value of $\sigma_o(\mathbf{Q}_k)$ with satisfying the constraint. The solution for $\sigma_o(\mathbf{Q}_k)$ is

$$\sigma_o(\mathbf{Q}_k) = \frac{\alpha_k \sigma_{w_k}^2}{\sigma_o(\mathbf{H}_k)\left\|\mathbf{u}_o(\mathbf{Q}_k)^H \mathbf{u}_o(\mathbf{H}_k)\right\|_2^2}. \tag{22}$$

Finally, $\mathbf{Q}_k$ can be obtained by its definition, i.e., $\mathbf{Q}_k = \sigma_o(\mathbf{Q}_k)\mathbf{u}_o(\mathbf{Q}_k)\mathbf{u}_o(\mathbf{Q}_k)^H$. The closed-form precoder $\mathbf{f}_k$ can then be given by

$$\mathbf{f}_k = \sqrt{\sigma_o(\mathbf{Q}_k)}\mathbf{u}_o(\mathbf{Q}_k). \tag{23}$$

3.3.2 Complexity Analysis of the Proposed Solution 3

We use Big O [6], denoted as $\mathcal{O}(\cdot)$, to calculate the complexity orders for the proposed Solution 3. First, let us define the complexity for some operations. Suppose that α is a scalar number. $\mathbf{X}$ and $\mathbf{Y}$ are respectively $p \times q$ and $q \times r$ matrices. As $p \ll q$ ($p \neq 1$) or $p = q$, the complexity order applying the SVD operation to $\mathbf{X}$ is of $\mathcal{O}(q^3)$. Additionally, for the scalar-matrix multiplication $\alpha\mathbf{X}$ and matrix multiplication $\mathbf{XY}$, their complexity orders are of $\mathcal{O}(pq)$ and $\mathcal{O}(pqr)$, respectively. According to above descriptions, the complexity orders for the proposed Solution 3 can be described as follows:

In the first step, we obtain the channel matrix $\mathbf{H}_k \in \mathbb{C}^{NM_t \times NM_t}$ via $\mathbf{H}_k = \mathbf{h}_k\mathbf{h}_k^H$ where $\mathbf{h}_k^H \in \mathbb{C}^{1\times NM_t}$. Its complexity is dominated by the matrix multiplication and thus is $\mathcal{O}((NM_t)^2)$. In the second step, we apply the SVD to the interference channel $\bar{\mathbf{H}}_k \in \mathbb{C}^{(K-1)\times NM_t}$ of the k-th UE for obtaining the null space $\mathbf{N}_k \in \mathbb{C}^{NM_t \times (NM_t-(K-1))}$, having the complexity $\mathcal{O}((NM_t)^3)$ of the SVD operation. In the third step, we apply the SVD to the channel matrix, $\mathbf{H}_k \in \mathbb{C}^{NM_t \times NM_t} = \sigma_o(\mathbf{H}_k)\mathbf{u}_o(\mathbf{H}_k)\mathbf{u}_o(\mathbf{H}_k)^H$, to obtain the first right singular vector $\mathbf{u}_o(\mathbf{H}_k) \in \mathbb{C}^{NM_t\times 1}$. Its complexity is also $\mathcal{O}((NM_t)^3)$ due to the SVD operation.

For the fourth step, according to Proposition 1, we need to calculate the equation $\mathbf{G}_k = \mathbf{N}_k^H\mathbf{u}_o(\mathbf{H}_k)\mathbf{u}_o(\mathbf{H}_k)^H\mathbf{N}_k$ to achieve $\mathbf{G}_k$. With $\mathbf{N}_k \in \mathbb{C}^{NM_t\times(NM_t-(K-1))}$ and $\mathbf{u}_o(\mathbf{H}_k) \in \mathbb{C}^{NM_t\times 1}$, we first define that $\mathbf{w}_k = \mathbf{N}_k^H\mathbf{u}_o(\mathbf{H}_k) \in \mathbb{C}^{(NM_t-(K-1))\times 1}$. The complexity of acquiring $\mathbf{w}_k$ is $\mathcal{O}(NM_t(NM_t-(K-1))) \approx \mathcal{O}((NM_t)^2)$. Then, we can obtain $\mathbf{G}_k$ by calculating $\mathbf{G}_k = \mathbf{w}_k\mathbf{w}_k^H$. This complexity is $\mathcal{O}((NM_t-(K-1))^2) \approx \mathcal{O}((NM_t)^2)$. Therefore, the complexity for this step is $\mathcal{O}(2(NM_t)^2)$.

In the fifth step, we apply the SVD to $\mathbf{G}_k \in \mathbb{C}^{(NM_t-(K-1))\times(NM_t-(K-1))}$ for getting the first right singular vector $\mathbf{v}_o(\mathbf{G}_k) \in \mathbb{C}^{(NM_t-(K-1))\times 1}$, whose complexity is $\mathcal{O}((NM_t-(K-1))^3) \approx \mathcal{O}((NM_t)^3)$. Then, in the sixth step, $\mathbf{u}_o(\mathbf{Q}_k)$ can be obtained by (21). Its complexity is caused by the matrix multiplication $\mathbf{u}_o(\mathbf{Q}_k) = \mathbf{N}_k\mathbf{v}_o(\mathbf{G}_k)$ and thus is $\mathcal{O}(NM_t(NM_t-(K-1))) \approx \mathcal{O}((NM_t)^2)$. For the seventh step, we can achieve $\sigma_o(\mathbf{Q}_k)$ utilizing (22). In this case, since α_k, $\sigma_{w_k}^2$, and $\sigma_o(\mathbf{H}_k)$ are the scalar numbers, the complexity is dominated by the norm operation. Additionally, because $\mathbf{u}_o(\mathbf{Q}_k)$ and $\mathbf{u}_o(\mathbf{H}_k)$ are column vectors $\in \mathbb{C}^{NM_t\times 1}$, the complexity of the norm operation is equal to that of the matrix multiplication and thus is $\mathcal{O}(NM_t)$. Finally, the precoder $\mathbf{f}_k$ for the k-th UE can be designed using (23). Its complexity is dominated by the scalar-matrix multiplication and thus is $\mathcal{O}(NM_t)$. Therefore, the complexity of obtaining each $\mathbf{f}_k$ is $\mathcal{O}(2NM_t + 4(NM_t)^2 + 3(NM_t)^3)$. Since there are totally K precoders in the system, the entire complexity of the proposed Solution 3 is $\mathcal{O}(2KNM_t + 4K(NM_t)^2 + 3K(NM_t)^3)$.

3.3.3 Convergence of the Three Proposed Solutions

In Subsections 3.1 and 3.2, the problem formulation can be rewritten as standard optimization problems such as SOCP and SDP. In this case, since they are both convex problems, and in our case, the SDP always leads to rank one symmetric PSD matrices, the corresponding solutions achieve the optimization, consequently guaranteeing the convergence.

For the proposed Solution 3, when the number NM_t of total transmit antennas is sufficiently larger than the number K of users, i.e., $NM_t \gg K$, it can achieve almost the same performance of SOCP and SDP. This is because when $NM_t \gg K$, the null space $\mathbf{N}_k \in \mathbb{C}^{NM_t \times (NM_t-(K-1))}$ of the interference channel $\bar{\mathbf{H}}_k \in \mathbb{C}^{(K-1)\times NM_t}$ gets closer to the space of $\mathbb{C}^{NM_t \times NM_t}$. Thus, the restriction on the solution space can be more relaxed, and the performance can more closely achieve the optimum one. Consequently, as the number NM_t of total transmit antennas is sufficiently large, the proposed Solution 3 obtains almost identical performance with SOCP and SDP, also confirming its convergence.

3.4 Proposed Phase Shifter Selection (PSS) Algorithm

Now let us move to the second step, which utilizes the precoding solutions introduced in Subsections 3.1–3.3 to turn off the phase shifters to reduce power consumption. Considering the precoding vector $\mathbf{f}_k$, the elements of $\mathbf{f}_k$ corresponding to small magnitudes are expected to have less effect on the results [17, 24], and can be turned off with only slight performance loss. Based on this idea, we propose a greedy algorithm which turns off a phase shifter corresponding to the smallest magnitude of $\mathbf{f}_k$, and this turn-off status will be sent back to obtain another precoding solution introduced in Subsections 3.1–3.3. This procedure repeats until the number of turn-off phase shifters leads to the minimum power consumption.

To represent the precoding solutions with turn-off phase shifters, we need to rewrite some equations in Subsections 3.1–3.3. We define a diagonal auxiliary matrix $\mathbf{A}_k^{(i)} \in \mathbb{C}^{NM_t \times NM_t}$ to represent the status of phase shifters connected to the k-th RF chain of each RRH at the i-th iteration. At the first iteration, we turn on all phase shifters connected to the k-th RF chain of each RRH by setting $\mathbf{A}_k^{(1)} = \mathbf{I}_{NM_t}$. Furthermore, setting $[\mathbf{A}_k^{(i)}]_{(n-1)M_t+m,(n-1)M_t+m} = 0$ means that the turn-off phase shifter is at the k-th RF chain to the m-th antenna of the n-th RRH at the i-th iteration. We add the auxiliary matrix to the proposed Solutions 1, 2, and 3 to control which elements in the designed precoder should be set to zeros.

3.4.1 Proposed PSS with Solution 1

For the proposed Solution 1, we introduce $\mathbf{A}_k^{(i)}$ to the problem in (10) to control which elements of $\mathbf{f}_k$ are set to zeros. We can rewrite the problem in (10) as

$$\begin{aligned} \underset{\{\{\mathbf{f}_{n,k}\}_{n=1}^{N}\}_{k=1}^{K}}{\text{minimize}} \quad & \sum_{n=1}^{N}\sum_{k=1}^{K} \|\mathbf{f}_{n,k}\|_2^2, \\ \text{s.t.} \quad & \sum_{k=1}^{K} \|\mathbf{f}_{n,k}\|_2^2 \le \mathcal{P}_n, \\ \mathrm{Re}(\mathbf{h}_k^H \mathbf{A}_k^{(i)} \mathbf{f}_k) \ge \sqrt{\alpha_k} & \Big\| [\mathbf{h}_k^H \mathbf{A}_1^{(i)} \mathbf{f}_1 \ \mathbf{h}_k^H \mathbf{A}_2^{(i)} \mathbf{f}_2 \ \cdots \ \mathbf{h}_k^H \mathbf{A}_{k-1}^{(i)} \mathbf{f}_{k-1} \\ & \mathbf{h}_k^H \mathbf{A}_{k+1}^{(i)} \mathbf{f}_{k+1} \ \cdots \ \mathbf{h}_k^H \mathbf{A}_K^{(i)} \mathbf{f}_K \ \sigma_{w_k}] \Big\|_2. \end{aligned} \tag{24}$$

It is worthwhile pointing out a fact that in (24), when some elements of $\mathbf{f}_k$ are zeros, these elements remain zeros after the iterations, which guarantees that the phase shifters can be turned off one after another until the minimum power consumption is attained. This fact is observed when we conduct the simulations via the CVX toolbox in MATLAB. Moreover, the second constraint in (24) determines the lower bound of precoder power consumption. If one sets some diagonal elements in $\mathbf{A}_k^{(i)}$ from 1 to 0 at the i-th iteration, the entries of $\mathbf{f}_k$ corresponding to the zero diagonal elements of $\mathbf{A}_k^{(i)}$ should have zero elements as well. This is because when $[\mathbf{A}_k^{(i)}]_{x,x} = 0$, $[\mathbf{A}_k^{(i)}\mathbf{f}_k]_x$ must also be zero, which makes $[\mathbf{f}_k]_x$ a redundant variable in (24). Hence, if the objective function is to minimize the total transmission power, $[\mathbf{f}_k]_x$ should remain zero to achieve the lowest power value.

After the problem in (24) is solved by one iteration, the problem to turn off the phase shifters becomes:

$$\begin{aligned} \underset{x,y}{\text{minimize}} \quad & \left| \begin{bmatrix} \mathbf{f}_1 & \mathbf{f}_2 & \cdots & \mathbf{f}_K \end{bmatrix}_{x,y} \right|, \\ \text{s.t.} \quad & \left| \begin{bmatrix} \mathbf{f}_1 & \mathbf{f}_2 & \cdots & \mathbf{f}_K \end{bmatrix}_{x,y} \right| > 0, \end{aligned} \tag{25}$$

where the problem in (25) is to find the position of a non-zero element, which has the minimum magnitude in the matrix $[\mathbf{f}_1 \quad \mathbf{f}_2 \quad \cdots \quad \mathbf{f}_K]$. After obtaining the solution of (25), one can set

$$\left[\mathbf{A}_{k=y}^{(i)}\right]_{x,x} = 0, \tag{26}$$

and then update $\mathbf{A}_k^{(i+1)}$ of the next iteration as follows:

$$\mathbf{A}_k^{(i+1)} = \mathbf{A}_k^{(i)}. \tag{27}$$

The following procedures are summarized to minimize the total power consumption P_{total} in (7) via turning off phase shifters for Solution 1.

- Step 1-1. Compute $\mathbf{f}_k$ by solving the problem in (24).
- Step 1-2. Find the phase shifter that needs to be turned off using (25).
- Step 1-3. Set zero element for $\mathbf{A}_k^{(i)}$ in (26) using the position (x, y) obtained in Step 1-2.
- Step 1-4. Update $\mathbf{A}_k^{(i+1)}$ for the next iteration using (27).

3.4.2 Proposed PSS with Solution 2

For the proposed Solution 2, $\mathbf{A}_k^{(i)}$ is utilized in a similar way as that for Solution 1. Thus, the problem in (14) is rewritten as follows:

$$\begin{aligned} \underset{\mathbf{Q}_1,\ \cdots,\ \mathbf{Q}_K}{\text{minimize}} \quad & \sum_{k=1}^{K} Tr(\mathbf{Q}_k), \\ \text{s.t.} \quad & Tr(\mathbf{H}_k \mathbf{A}_k^{(i)} \mathbf{Q}_k {\mathbf{A}_k^{(i)}}^H) - \alpha_k \sum_{l \neq k}^{K} Tr(\mathbf{H}_k \mathbf{A}_l^{(i)} \mathbf{Q}_l {\mathbf{A}_l^{(i)}}^H) \geq \alpha_k \sigma_{w_k}^2, \\ & \mathbf{Q}_k \succeq 0. \end{aligned} \tag{28}$$

After $\mathbf{Q}_k$ is solved in (28), $\mathbf{f}_k$ can be obtained and then one can determine which elements of $\mathbf{f}_k$ should be set to zeros via $\mathbf{A}_k^{(i)}$ like the procedures for Solution 1. We summarize the procedures that minimize the total power consumption P_{total} in (7) for Solution 2 as follows:

- Step 2-1. Compute $\mathbf{f}_k$ by solving the problem in (28).
- Step 2-2. Find the phase shifter that needs to be turned off using (25).
- Step 2-3. Set zero element for $\mathbf{A}_k^{(i)}$ in (26) using the position (x, y) obtained in Step 2-2.
- Step 2-4. Update $\mathbf{A}_k^{(i+1)}$ for the next iteration using (27).

3.4.3 Proposed PSS with Solution 3

For the proposed solution 3, $\mathbf{A}_k^{(i)}$ is again used to control which elements of $\mathbf{f}_k$ should be set to zeros. However, this matrix should be applied in (17) and

(18) when one determines the interference channel and its null space, which are rewritten as follows:

$$\bar{\mathbf{H}}_k = \left[\mathbf{A}_k^{(i)H}\mathbf{h}_1 \ \mathbf{A}_k^{(i)H}\mathbf{h}_2 \ \cdots \ \mathbf{A}_k^{(i)H}\mathbf{h}_{k-1} \ \mathbf{A}_k^{(i)H}\mathbf{h}_{k+1} \ \cdots \ \mathbf{A}_k^{(i)H}\mathbf{h}_K \right]^H. \quad (29)$$

and

$$\mathbf{u}_o(\mathbf{Q}_k) = \mathbf{A}_k^{(i)}\mathbf{N}_k\mathbf{x}_k. \quad (30)$$

Through (29) and (30), one can obtain $\mathbf{f}_k$ by using the proposed Solution 3 and then find which elements of $\mathbf{f}_k$ should be set to zeros. Therefore, we summarize the procedures to minimize the total power consumption P_{total} in (7) in the following steps.

- Step 3-1. Compute $\mathbf{f}_k$ applying (29) and (30) to (20)–(23).
- Step 3-2. Find the phase shifter that needs to be turned off using (25).
- Step 3-3. Set zero element for $\mathbf{A}_k^{(i)}$ in (26) using the position (x, y) obtained in Step 3-2.
- Step 3-4. Update $\mathbf{A}_k^{(i+1)}$ for the next iteration using (27).

4 Simulation Results

In this section, simulation results are provided to show the performance of the proposed system and algorithms. In these experiments, the propagation channel model in [3] is used, which is between the n-th RRH and the k-th UE. There are 6 paths and each path angle $\theta_{l,k,n}$ is assumed to be uniformly distributed. The complex gain of each path is assumed to be $\alpha_{l,k,n} \sim \mathcal{CN}(0, 1)$. We assume that the inter-element spacing d of array antenna is half-wavelength and the background noise power is -101 dBm. For the path loss model, the alpha-beta-gamma (ABG) model is used [7, 22], which is a distance and frequency dependent model with path loss being modeled as $\text{PL[dB]} = 10\alpha \log_{10}(d_{n,k}) + \beta + 10\gamma \log_{10}(f) + X_\sigma$. It models an urban microcellular open square scenario, where the related parameters are summarized in Table 1.

4.1 Experiment 1: Differences among Three Proposed Solutions

In this experiment, we would like to see how similar the three proposed solutions are in terms of magnitude and phase. We compared the precoding matrices of the first RRH obtained through the three different solutions mentioned in Section 3 without the phase shifter selection algorithm. In this case, all phase shifters are turned on.

Algorithm 1 : Proposed Phase Shifter Selection Algorithm

Input: The number of UEs K; The number of RRHs N; The number of transmit antennas M_t; The number of RF chains $N_{RF} = K$; The noise power $\sigma_{w_k}^2$; The channels of all UEs $\mathbf{h}_1, \mathbf{h}_2, \cdots, \mathbf{h}_K$; The number of turn-off phase shifters C, where $C \leq N \cdot N_{RF} \cdot M_t$.

Output: The proposed analog precoders $\mathbf{F}_n$, $\forall n = 1, 2, \cdots, N$, and the set of active phase shifters.

Initialization: $i = 1$, $\mathbf{A}_k^{(i)} = \mathbf{I}_{NM_t}$, $\forall k = 1, 2, \cdots, N_{RF}$, and $P_{total}^{(i)} = \infty$.
for $i = 1 : C$ **do**
    Compute $\mathbf{f}_k$, $\forall k = 1, 2, \cdots, K$, using Step 1-1 if Solution 1 is to be used; or using Step 2-1 if Solution 2 is to be used; or using Step 3-1 if Solution 3 is to be used.
    Obtain $\mathbf{F}_n^{(i)}$, $\forall n = 1, 2, \cdots, N$, via $\mathbf{f}_k$ obtained in Step 3.
    Compute the total power consumption P_{total} in (7).
    $P_{total}^{(i+1)} = P_{total}$.
    if $P_{total}^{(i)} < P_{total}^{(i+1)}$
        break;
    else
        Compute (x, y) using (25).
        Set zero element for $\mathbf{A}_k^{(i)}$ using (26).
        Update $\mathbf{A}_k^{(i+1)}$ using (27).
        $\mathbf{F}_n = \mathbf{F}_n^{(i)}$, $\forall n = 1, 2, \cdots, N$.
        The non-zero elements in $\text{diag}(\mathbf{A}_k^{(i)})$, $\forall k = 1, 2, \cdots, K$, correspond to the set of active phase shifters.
    end if
end for

Table 1: The related parameters.

Parameters	Values
Number of UEs K	3
Number of RRHs N	3
Number of BBU	1
Carrier frequency f	60 GHz
Gaussian random variable X_σ	$\sim \mathcal{N}(0, 7.8)$
Distance between the k-th UE and n-th RRH $d_{n,k}$	100 m
Dependence of path loss on distance α	4.4
Optimized offset value for path loss β	2.4 dB
Dependence of path loss on frequency γ	1.9

We show the magnitude and phase of each element in the precoding matrices of the first RRH. Let the target rate of each UE be 3 bits/s/Hz. Figure 3 shows the results for $M_t = 4$, and Figure 4 shows those for $M_t = 16$. The horizontal axes of the figures represent the element index in the precoders of the first RRH, which are corresponding to the three UEs such as $\mathbf{f}_{1,1}, \mathbf{f}_{1,2}$, and $\mathbf{f}_{1,3}$ defined in (1). Moreover, the vertical axes of the two figures respectively represent the magnitude and phase of each element in the precoders.

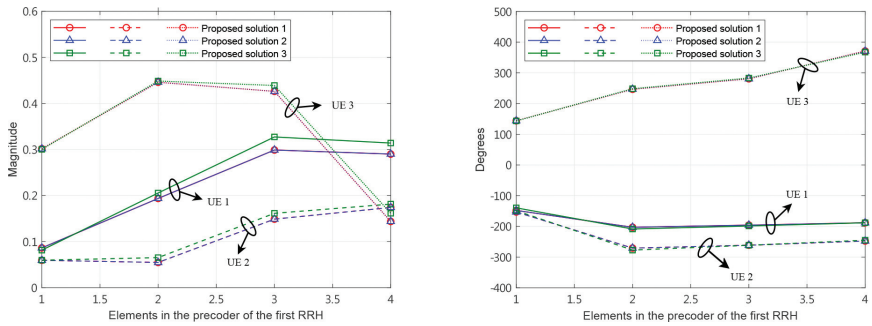

Figure 3: Comparison of the precoders obtained by the three proposed solutions with $M_t = 4$.

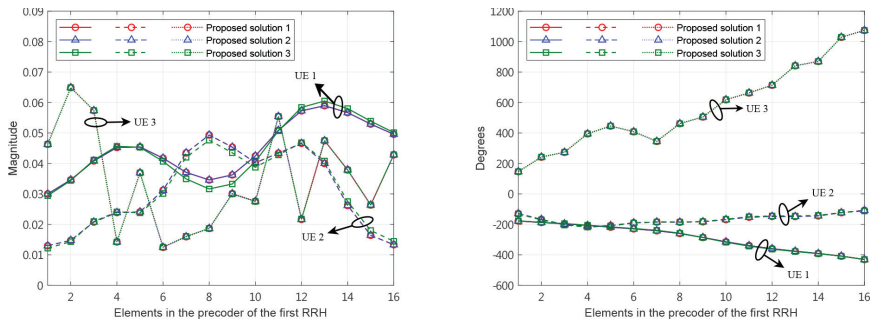

Figure 4: Comparison of the precoders obtained by the three proposed solutions with $M_t = 16$.

We have the following observations: First, from the two figures, the magnitudes and phases of the precoders obtained via the proposed three solutions are very close. This means that similar solutions can be obtained via the two proposed optimization methods (Solutions 1 and 2) as well as the proposed closed-form method (Solution 3). Also, it implies that although the three proposed methods tackle the same problem via three different view points, they all lead to similar results. Hence it validates the correctness of the proposed solutions implicitly. Moreover, as the number of antennas M_t increases, e.g.,

from 4 to 16, the similarity of the three proposed solutions becomes more pronounced. From Figure 4, the magnitude and phase of the precoders using the proposed Solution 3 are significantly close to those of Solutions 1 and 2 having the convergence, verifying that the proposed Solution 3 also achieves the convergence.

The observations provide useful insight in implementations. That is, although Solutions 1 and 2 theoretically approach the optimal performance because the problem is solved numerically by the interior-point method, the corresponding computational complexity is high compared to that of Solution 3. Since the three solutions lead to similar results, one can select the one that has the smallest complexity in this circumstance.

4.2 Experiment 2: Performance Comparison of the Proposed Solutions

From Experiment 1, we learn that the three proposed solutions have only slight differences. In this experiment, we verify whether such phenomenon leads to close performance in terms of transmission power defined in (6) or not. Again let all the phase shifters be active, and the target rate of each UE be 3 bits/s/Hz. Figure 5 shows the transmission power, $\sum_{n=1}^{N} \frac{1}{\eta_n} \|\mathbf{F}_n\|_F^2$ with $\frac{1}{\eta_n} = 2.8$, as functions of number of transmit antennas for the three proposed solutions. From the figure, the three solutions indeed have similar transmission power. Moreover, performance similarity between the proposed Solution 3 and other two becomes more pronounced as the number of transmit antennas increases. Similar to the above discussion, the convergence of the proposed Solution 3 becomes more pronounced as well.

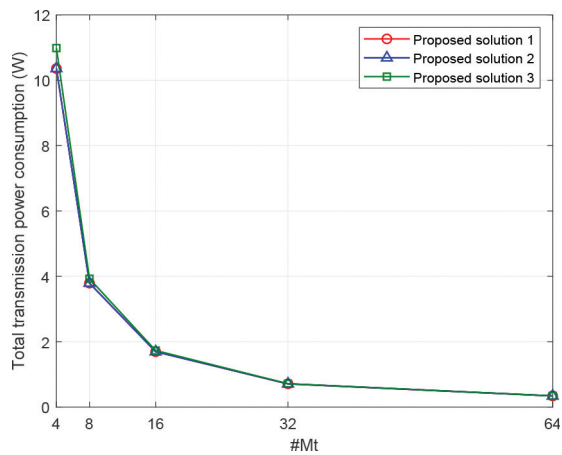

Figure 5: Comparison of transmission power among Solutions 1, 2, and 3 for $M_t = 4, 8, 16, 32,$ and 64.

4.3 *Experiment 3: Power Reduction via Proposed Solutions and Algorithm 1*

In this experiment, we show the reduction of power consumption using the proposed scheme. From Experiments 1 and 2, the three proposed precoding solutions have similar results. Hence here we use Solution 3 for the precoding solution for complexity reduction and together utilize Algorithm 1 to switch off phase shifters for power reduction. The results are compared to those without turning off phase shifters.

According to [14], we set two commonly adopted power consumption of phase shifters. One is each active phase shifter consumes $P_{PS} = 30$ mW and the other is $P_{PS} = 10$ mW. Let $P_{RF} = 300$ mW as suggested in [11] and the number of antennas be $M_t = 64$.

Figure 6 shows (a) the power consumption and (b) the number of turn-off phase shifters as functions of target rate for $P_{PS} = 10$ mW; moreover, Figure 7 shows those for $P_{PS} = 30$ mW, where the solid curves are for $\frac{1}{\eta_n} = 4$ and the dash curves are for $\frac{1}{\eta_n} = 2.8$. We have several observations: First, the power consumption can be significantly reduced by the proposed precoding solution and turning off phase shifters in Algorithm 1. For example, in Figure 7 and when the target rate is 3 bits/s/Hz, the power consumption is up to around 20 W (see the triangular curves) without proposed methods but it is significantly reduced to around 5 W (see the rectangular curves) with the proposed schemes by turning off around 178 phase shifters.

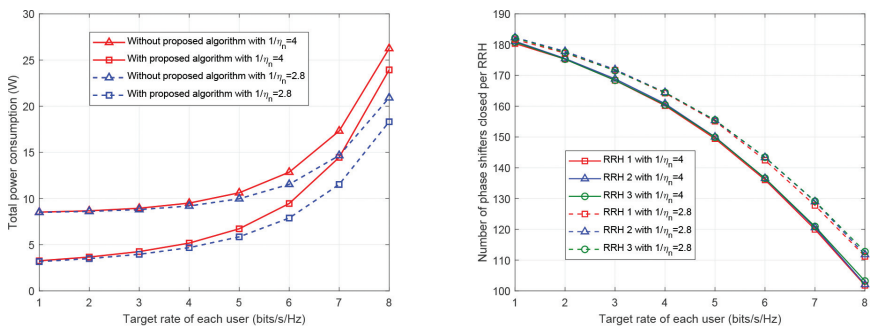

(a) Total power consumption.

(b) Number of turn-off phase shifters at each RRH.

Figure 6: Comparisons of power consumption and the number of turn-off phase shifters with $M_t = 64$ and $P_{PS} = 10$ mW.

Second, from Figures 6 and 7, the power reduction is more pronounced when P_{PS} increases from 10 to 30 mW. This can be seen from the increased performance gap between the systems with and without the proposed schemes. For example, when the target rate is 3 bits/s/Hz, the gap is around $9 - 4 = 5$ W in Figure 6, while it is around $20 - 5 = 15$ W in Figure 7.

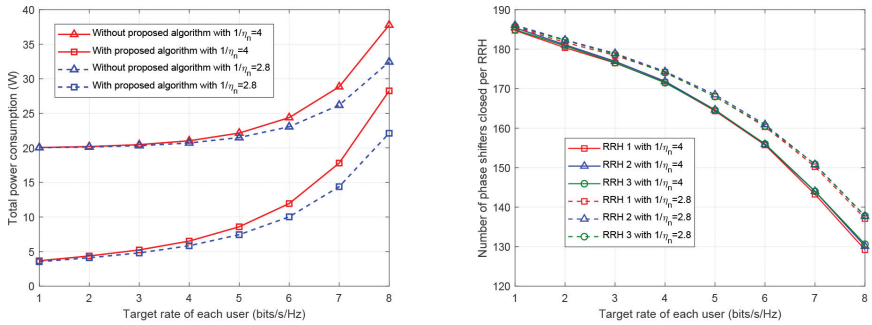

(a) Total power consumption.

(b) Number of turn-off phase shifters at each RRH.

Figure 7: Comparisons of power consumption and the number of turn-off phase shifters with $M_t = 64$ and $P_{PS} = 30$ mW.

Third, $\frac{1}{\eta_n} = 2.8$ implies that the power consumption from power amplifier is relatively low compared to the hardware power consumption. On the other hand, $\frac{1}{\eta_n} = 4$ implies that the power consumption from power amplifier is relatively high. Therefore, as η_n decreases, the impact of transmission power increases, which reduces power that can be saved using Algorithm 1.

Finally, when the target rate increases, the advantages of using the proposed scheme decreases since the performance gap reduces and the corresponding number of turn-off phase shifters decreases, observed from the two figures when target rate increases from 1 to 8 bits/s/Hz. This is not surprising because when the target rate increases, beamforming becomes important to concentrate the received gain to support high target rate. In this case, most phase shifters should be turned on to form desired beam patterns.

4.4 Experiment 4: Comparison of Computational Complexity for Proposed Schemes

In this experiment, we compare the computational complexity for the three proposed algorithms in Section 3 together with Algorithm 1. We evaluate the computational time for comparison purpose.

To obtain the results, we use a desktop PC embedded with an Intel i5-9600K CPU operating at 3.7 GHz, 6 GB RAM, and CVX toolbox in MATLAB R2019a. Let the target rate of each UE be 3 bits/s/Hz. We calculate the average computational time in each realization when the phase shifters are turned off by 33 percent. This means that when the number of transmit antennas at each RRH is 4, 8, 16, 32, and 64, we have to turn off 12, 24, 48, 96, and 192 phase shifters in the system, respectively, where the total number of phase shifters used is $N \cdot N_{RF} \cdot M_t$.

Figure 8 shows the average time as a function of the number of transmit antennas. Note that when $M_t \geq 64$, the computational time for Solution 2

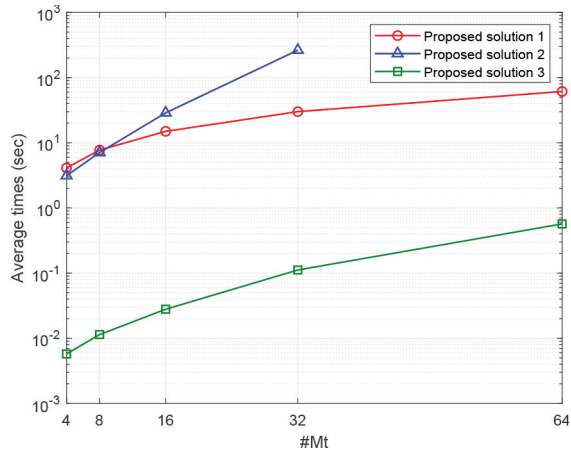

Figure 8: Comparison of computational complexity among the proposed three solutions with $M_t = 4, 8, 16, 32$, and 64.

(the proposed SDR-based solution) reaches a limit and thus the result is not included in this figure.

From the figure, we see that Solution 3 indeed demands much lower computational complexity than other two solutions. The gap is up to around 100-time! This result is reasonable because Solution 3 is a closed-form solution while others obtain the results numerically. Thus, with the discussions in Experiments 1 and 2, Solution 3 achieves similar results and performance with other two optimization methods, but its computational complexity is much lower than other two schemes. As a result, it is a potential solution when implementation issues are considered in practice.

4.5 Experiment 5: Effects on Beam Patterns for Turning Off Phase Shifters via Wireless InSite

In this experiment, we evaluate how the beam patterns are changed when the phase shifters are turned off. This is to see whether or not the resulting beam pattern still points to the UEs and its rationality to turn off the phase shifters in practical applications.

We use a ray tracing tool named Wireless InSite [28], which can generate simulated wireless channels when the geometrical configurations are properly set. Referring to Figure 9, we create an indoor environment which has three UEs and three RRHs in a 40×60 space (m^2) with the zero-reflection concrete walls. Each RRH has a ULA antenna with 16 elements and 3 RF chains. The waveform type is sinusoid. In this case, there are totally 144 phase shifters. The carrier frequency is 28 GHz, and the element distance of the array antenna is

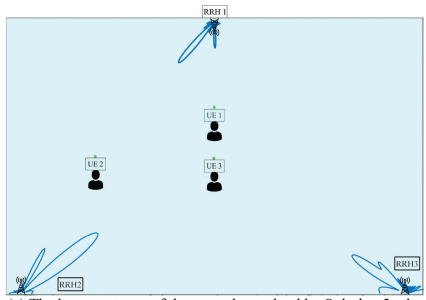

(a) The beam patterns of the precoders solved by Solution 3 when all phase shifters are opened.

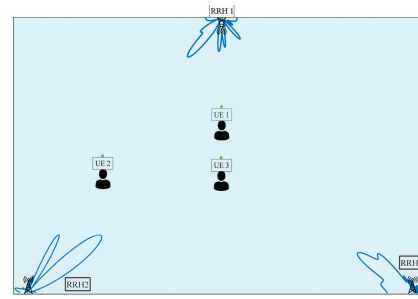

(b) The beam patterns of the precoders solved by Solution 3 when 72 phase shifters are turned off.

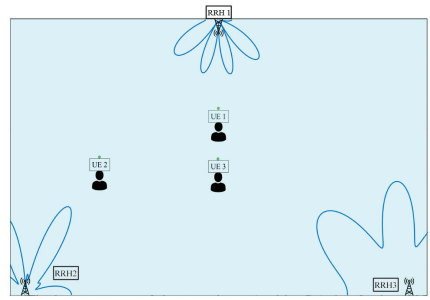

(c) The beam patterns of the precoders solved by Solution 3 when 135 phase shifters are turned off.

Figure 9: The beam patterns of the precoders solved by Solution 3.

half-wavelength. The target rate of each UE is 3 bits/s/Hz. The wireless channels are created by the Wireless InSite 3.3, and we use the channels to calculate the precoding solution in Solution 3 and turn off the phase shifters using Algorithm 1. The corresponding beam patterns are generated and drawn in Figure 9.

Figures 9(a), (b), and (c) show the beam patterns that turn off (a) 0, (b) 72, and (c) 135 phase shifters when the phase shifter consumes $P_{PS} = 30$ mW and $\frac{1}{\eta_n} = 2.8$. From Figure 9 (a), when there is no phase shifter turned off, the formed beams from the three RRHs are concentrated and point directly to the three UEs. Then, in Figure 9(b), when around 50% phase shifters are turned off, the resulting beams still reasonably point to the UEs. However to achieve the same target rate, the beam widths become larger. Finally, when 93% phase shifters are turned off in Figure 9(c), the resulting beam patterns are much smoother, wider, and more non-directional than those in Figures 9(a) and (b). Nevertheless, since the target rate is low and is only 3 bits/s/Hz, the requirement for shaping beam patterns is not mandatory. Moreover, although the beams become wider, which seems to cause more power consumption, the power consumption can be actually significantly reduced because of turning off most of the phase shifters, such as shown in Experiment 3.

4.6 *Experiment 6: Performance Improvement of the Proposed System with Postcoder via Wireless InSite*

This experiment follows Experiment 5 and uses the same parameter settings except the number of user antennas. To reflect a realistic situation of current handsets, each user is equipped with 4-element ULA antenna instead of a single antenna. Consequently, the postcoding effects can be considered to improve the performance of the proposed system. In this experiment, we design each user's postcoder using the maximum ratio combining (MRC) by taking the first left singular vector corresponding to the largest singular value of the entire channel viewed from the user.

Similar to Experiment 5, the proposed Solution 3 and Algorithm 1 are adopted to respectively obtain the precoding results and further turn off the phase shifters. Figure 10 shows the transmit and receive beam patterns of the proposed system when almost all phase shifters of the RRHs are turned off. From the figure, each user has the receive beam pattern pointing to the relatively importaint RRHs. For example, UEs 1 and 2 respectively direct their beamformings to RRHs 1 and 2. UE 3 generates the receive beams simultaneously towards RRHs 2 and 3. With these postcoding gains, each user achieves the target rate more easily, consequently requiring fewer phase shifters at the RRHs. In this case, 141 phase shifters (98% of all phase shifters) can be turned off, in which only one phase shifter is turned on at RRH 1, causing an isotropic transmit beamforming. Further, RRH 3 can be completely closed. Additionally, the number of turn-off phase shifters is more than that in Experiment 5 (135 phase shifters are turned off).

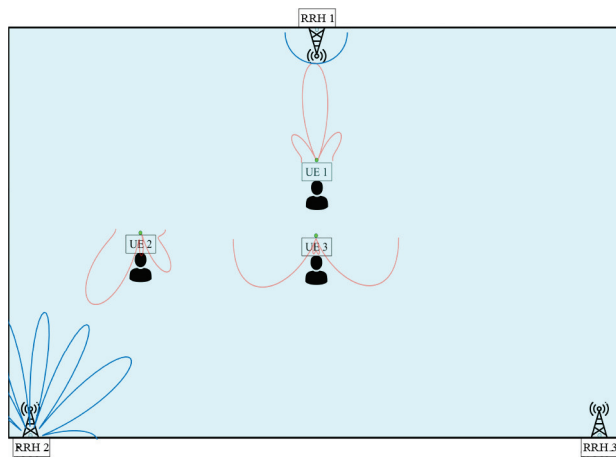

Figure 10: The beam patterns of the proposed system when 141 phase shifters are turned off.

5 Conclusion

We have proposed three different solutions to design the C-RAN beamforming to minimize the power consumption under fixed user target rates. Within the three solutions, the third solution does not need to use optimization toolbox and can significantly reduce the computational complexity; meanwhile it also achieves almost the same numerical results with other two optimization methods when the number of antennas is sufficiently large. Based on the beamforming solutions, we have proposed algorithms to select and turn off phase shifters to further greatly reduce the power consumption. Simulation results have shown that under fixed user target rates, many phase shifters can be turned off and total power consumption can be indeed significantly decreased by the proposed schemes. The feasibility and practice of the proposed solutions have also been verified by the ray tracing tool Wireless Insite.

Appendix

Proof of Lemma 1

Proof. From (10), the constraint can be transformed into the following equation:

$$|\mathbf{h}_k^H \mathbf{f}_k| \geq \sqrt{\alpha_k} \cdot \sqrt{\left(\sum_{l \neq k}^{K} |\mathbf{h}_k^H \mathbf{f}_l|^2 + \sigma_{w_k}^2 \right)}. \tag{31}$$

Furthermore, we utilize the l_2-norm interpretation in the matrix norm theorem, which allows us to rewrite (31) as

$$|\mathbf{h}_k^H \mathbf{f}_k| \geq \sqrt{\alpha_k} \left\| [\mathbf{h}_k^H \mathbf{f}_1 \ \mathbf{h}_k^H \mathbf{f}_2 \ \cdots \ \mathbf{h}_k^H \mathbf{f}_{k-1} \ \mathbf{h}_k^H \mathbf{f}_{k+1} \ \cdots \ \mathbf{h}_k^H \mathbf{f}_K \ \sigma_{w_k}] \right\|_2. \tag{32}$$

Observe that the optimal value of the problem in (10) does not change if the phase of the optimal solution changes. Hence, one can rotate the phase of the solution arbitrarily, i.e., $\mathbf{f}_k \cdot e^{-j\theta_k}$, so that the left side of (32) is on the real number axis, i.e., $\mathrm{Im}(\mathbf{h}_k^H \mathbf{f}_k) = 0$. When $\mathrm{Im}(\mathbf{h}_k^H \mathbf{f}_k) = 0$, it yields $|\ \mathbf{h}_k^H \mathbf{f}_k| = \mathrm{Re}(\mathbf{h}_k^H \mathbf{f}_k)$. Hence, (32) can be rewritten as (11).

Below we assume that $\mathbf{f}_{n,k}^{opt}$ is the optimal solution and prove that $\mathbf{f}_{n,k}^{opt} \cdot e^{-j\theta_k}$ has no effect on the problem in (10). First we focus on its objective function, which can be expressed as

$$\begin{aligned} \sum_{n=1}^{N} \sum_{k=1}^{K} \left\| \mathbf{f}_{n,k}^{opt} \cdot e^{-j\theta_k} \right\|_2^2 &= \sum_{n=1}^{N} \sum_{k=1}^{K} \left(e^{j\theta_k} \cdot \mathbf{f}_{n,k}^{opt\,H} \mathbf{f}_{n,k}^{opt} \cdot e^{-j\theta_k} \right) \\ &= \sum_{n=1}^{N} \sum_{k=1}^{K} \left\| \mathbf{f}_{n,k}^{opt} \right\|_2^2. \end{aligned} \tag{33}$$

As we have seen, the optimal solution multiplied by an angle has no effect on the objective function. Second, we consider the constraints of the problem in (10), which can be expressed as

Constraint 1 :

$$\begin{aligned}\sum_{k=1}^{K}\left\|\mathbf{f}_{n,k}^{opt}\cdot e^{-j\theta_k}\right\|_2^2 \le \mathcal{P}_n &\Rightarrow \sum_{k=1}^{K}\left(e^{j\theta_k}\cdot \mathbf{f}_{n,k}^{opt\,H}\mathbf{f}_{n,k}^{opt}\cdot e^{-j\theta_k}\right)\le \mathcal{P}_n \\ &\Rightarrow \sum_{k=1}^{K}\left\|\mathbf{f}_{n,k}^{opt}\right\|_2^2 \le \mathcal{P}_n.\end{aligned} \tag{34}$$

Constraint 2 :

$$\begin{aligned}\left|\mathbf{h}_k^H\mathbf{f}_k^{opt}\cdot e^{-j\theta_k}\right|^2 &\ge \alpha_k\left(\sum_{l\neq k}^{K}\left|\mathbf{h}_k^H\mathbf{f}_l^{opt}\cdot e^{-j\theta_l}\right|^2+\sigma_{w_k}^2\right)\\ &\Rightarrow \left(e^{j\theta_k}\cdot \mathbf{f}_k^{opt\,H}\mathbf{h}_k\mathbf{h}_k^H\mathbf{f}_k^{opt}\cdot e^{-j\theta_k}\right)\\ &\ge \alpha_k\left(\sum_{l\neq k}^{K}\left(e^{j\theta_l}\cdot \mathbf{f}_l^{opt\,H}\mathbf{h}_k\mathbf{h}_k^H\mathbf{f}_l^{opt}\cdot e^{-j\theta_l}\right)+\sigma_{w_k}^2\right)\\ &\Rightarrow \left|\mathbf{h}_k^H\mathbf{f}_k^{opt}\right|^2 \ge \alpha_k\left(\sum_{l\neq k}^{K}\left|\mathbf{h}_k^H\mathbf{f}_l^{opt}\right|^2+\sigma_{w_k}^2\right),\end{aligned} \tag{35}$$

where $\mathbf{f}_k^{opt}=[\mathbf{f}_{1,k}^{opt\,T}\quad \mathbf{f}_{2,k}^{opt\,T}\quad \cdots\quad \mathbf{f}_{N,k}^{opt\,T}]^T\in\mathbb{C}^{NM_t\times 1}$ is the same as (3). At present, we have also proved that the optimal solution multiplied by an angle has no effect on the constraints. Thus, we can find an angle, i.e., $\theta_k=\angle\,\mathbf{h}_k^H\mathbf{f}_k^{opt}$, such that $\mathbf{h}_k^H\mathbf{f}_k^{opt}\cdot e^{-j\theta_k}=\mathrm{Re}(\mathbf{h}_k^H\mathbf{f}_k^{opt}\cdot e^{-j\theta_k})$. □

Proof of Proposition 1

Proof. Using the property that $Tr(a\cdot\mathbf{X})=a\cdot Tr(\mathbf{X})$, the constraint in (19) can be rewritten as

$$\sigma_o(\mathbf{H}_k)\sigma_o(\mathbf{Q}_k)Tr(\mathbf{u}_o(\mathbf{H}_k)\mathbf{u}_o(\mathbf{H}_k)^H\mathbf{N}_k\mathbf{x}_k(\mathbf{N}_k\mathbf{x}_k)^H)\ge\alpha_k\sigma_{w_k}^2. \tag{36}$$

We can see that both $\sigma_o(\mathbf{H}_k)$ and $\alpha_k\sigma_{w_k}^2$ are the fixed constants. Therefore, by maximizing the trace term in (36), the minimum value of $\sigma_o(\mathbf{Q}_k)$ can be obtained to achieve the minimum transmit power in (19). Hence, we need to find the best linear combination of the null space that maximizes the trace

term. For this reason, we start with the following problem.

$$\begin{aligned} \underset{\mathbf{x}_k}{\text{maximize}} \quad & Tr(\mathbf{u}_o(\mathbf{H}_k)\mathbf{u}_o(\mathbf{H}_k)^H\mathbf{N}_k\mathbf{x}_k(\mathbf{N}_k\mathbf{x}_k)^H), \\ \text{s.t.} \quad & \|\mathbf{N}_k\mathbf{x}_k\|_2^2 = 1. \end{aligned} \tag{37}$$

The optimal solution to the problem in (37) can be derived below: Using the property that $Tr(\mathbf{AB}) = Tr(\mathbf{BA})$ and $Tr(a) = a$, $\forall a \in \mathbb{C}^{1\times 1}$, the objective function of the problem in (37) can be reformulated as

$$\underset{\mathbf{x}_k}{\text{maximize}}\ \mathbf{x}_k^H\mathbf{N}_k^H\mathbf{u}_o(\mathbf{H}_k)\mathbf{u}_o(\mathbf{H}_k)^H\mathbf{N}_k\mathbf{x}_k. \tag{38}$$

Now let us move to the constraint in (37). From the definition of $\mathbf{N}_k$, we can observe that $\mathbf{N}_k^H\mathbf{N}_k = \mathbf{I}$. Then, the constraint in (37) can be reformulated as

$$\|\mathbf{x}_k\|_2^2 = 1. \tag{39}$$

Using (38) and (39) and letting $\mathbf{G}_k = \mathbf{N}_k^H\mathbf{u}_o(\mathbf{H}_k) \cdot \mathbf{u}_o(\mathbf{H}_k)^H\mathbf{N}_k$, we can reformulate the problem in (37) as

$$\begin{aligned} \underset{\mathbf{x}_k}{\text{maximize}} \quad & \mathbf{x}_k^H\mathbf{G}_k\mathbf{x}_k, \\ \text{s.t.} \quad & \|\mathbf{x}_k\|_2^2 = 1. \end{aligned} \tag{40}$$

We can easily recognize $\mathbf{G}_k$ as a Hermitian matrix. Therefore, the problem in (40) is the well-known Rayleigh quotient problem and its optimal solution is equivalent to $\mathbf{x}_k = \mathbf{v}_o(\mathbf{G}_k)$ [8], where $\mathbf{v}_o(\mathbf{G}_k)$ is the eigenvector corresponding to the largest eigenvalue of $\mathbf{G}_k$. □

Biographies

Chi-Chen Wang received the M.S. degree from the Institute of Electrical and Control Engineering, National Chiao Tung University (now National Yang Ming Chiao Tung University, NYCU), Hsinchu, Taiwan, in 2021. His research interest includes signal processing for wireless communications.

Yan-Yin He received the M.S. degree from the Institute of Electrical and Control Engineering, National Chiao Tung University (now National Yang Ming Chiao Tung University, NYCU), Hsinchu, Taiwan, in 2019, where he is currently pursuing the Ph.D. degree.

His research interests include signal processing and transceiver beamforming design for the mmWave communications. He was selected as an Honorary Member of the Phi Tau Phi Scholastic Honor Society in 2018. He was awarded the Scholarship from the Institute of Electrical and Control Engineering, NYCU, in 2019, and the scholarships of Pan Wen-Yuan Foundation in both 2020 and 2021.

Shang-Ho (Lawrence) Tsai (Senior Member, IEEE) received the Ph.D. degree in electrical engineering from the University of Southern California (USC), USA, in August 2005. From June 1999 to July 2002, he was with Silicon Integrated Systems Corporation (SiS), where he participated the VLSI design for DMT-ADSL systems. From September 2005 to January 2007, he was with MediaTek Inc. (MTK) participating in the VLSI design for MIMO-OFDM systems and standard specifications for IEEE 802.11n. Since February 2007, he has been with the Department of Electrical Engineering, National Chiao Tung University (now National Yang Ming Chiao Tung University), where he is currently a Professor. From June 2013 to December 2013, he was a Visiting Fellow with the Department of Electrical Engineering, Princeton University. His research interests are in the areas of signal processing for communications, statistical signal processing, and machine learning. He was in the Editorial Board of IEEE SigPort from 2018 to 2020. He has been an Editor of *APSIPA Transactions on Signal and Information Processing* since 2022. He is in the Signal Processing for Communications and Networking Technical Committee (SPCOM TC) of IEEE Signal Processing Society in 2023–2025.

He was awarded a Government Scholarship for Overseas Study from the Ministry of Education, Taiwan, from 2002 to 2005. He was awarded the Micron Teacher Award at 2018. He is a distinguished lecturer in the APSIPA in 2022–2023.

Acknowledgment

The authors would like to thank all the anonymous reviewers for their constructive suggestions, which have significantly improved the quality of this work.

Financial Support

This research was supported by the Ministry of Science and Technology (MOST), Taiwan under Grant MOST 110-2221-E-A49-02 and Grant MOST 109-2221-E-009-106.

References

[1] Z. Al-Abbasi, K. Rabie, and D. So, "EE Optimization for Downlink NOMA-based Multi-tier CRANs," *IEEE Trans. Veh. Technol.*, 70, 2021, 5880–91.

[2] Anokiwave, "AWMF-0108 Developer Kit Product Overview," 2018, http://www.anokiwave.com/specifications/AWMF-0108-DK.pdf (accessed on 09/04/2018).

[3] O. E. Ayach, S. Rajagopal, S. Abu-Surra, Z. Pi, and R. Heath, "Spatially Sparse Precoding in Millimeter Wave MIMO Systems," *IEEE Transactions on Wireless Communications*, 13, 2014, 1499–513.

[4] B. Dai and W. Yu, "Energy Efficiency of Downlink Transmission Strategies for Cloud Radio Access Networks," *IEEE Journal on Selected Areas in Communications*, 34, 2016, 1037–50.

[5] X. Gao, L. Dai, S. Han, C.-L. I, and R. Heath, "Energy-efficient Hybrid Analog and Digital Precoding for mmWave MIMO Systems with Large Antenna Arrays," *IEEE Journal on Selected Areas in Communications*, 34, 2016, 998–1009.

[6] G. Golub and C. F. Van Loan, *Matrix Computations*, 3rd ed, Baltimore, MA: The Johns Hopkins University Press, 1996.

[7] V. Ha, D. Nguyen, and J.-F. Frigon, "System Energy-efficient Hybrid Beamforming for mmWave Multi-user Systems," *IEEE Transactions on Green Communications and Networking*, 4, 2020, 1010–23.

[8] R.-A. Horn and C.-R. Johnson, *Matrix Analysis*, Cambridge: Cambridge University Press, 1985.

[9] A. Iqbal, M.-L. Tham, and Y. Chang, "Double Deep Q-network-based Energy-efficient Resource Allocation in Cloud Radio Access Network," *IEEE Access*, 9, 2021, 20440–9.

[10] J. Kim, S.-H. Park, O. Simeone, I. Lee, and S. Shamai Shitz, "Joint Design of fronthauling and Hybrid Beamforming for Downlink C-RAN Systems," *IEEE Transactions on Communications*, 67, 2019, 4423–34.

[11] Y. Lu, C. Cheng, J. Yang, and G. Gui, "Improved Hybrid Precoding Scheme for mmWave Large-scale MIMO Systems," *IEEE Access*, 7, 2019, 12027–34.

[12] Z.-Q. Luo, W.-K. Ma, A.-C. So, Y. Ye, and S. Zhang, "Semidefinite Relaxation of Quadratic Optimization Problems," *IEEE Signal Processing Mag.*, 27, 2010, 20–34.

[13] C. Masouros, M. Sellathurai, and T. Ratnarajah, "Computationally Efficient Vector Perturbation Precoding using Thresholded Optimization," *IEEE Transactions on Communications*, 61, 2013, 1880–90.

[14] R. Mendez-Rial, C. Rusu, N. Gonzalez-Prelcic, A. Alkhateeb, and R. W. Heath, "Hybrid MIMO Architectures for Millimeter Wave Communications: Phase Shifters or Switches?" *IEEE Access*, 4, 2016, 247–67.

[15] C. Pan, M. Elkashlan, J. Wang, J. Yuan, and L. Hanzo, "User-centric C-RAN Architecture for Ultra-dense 5G Networks: Challenges and Methodologies," *IEEE Transactions on Communications*, 56, 2018, 14–20.

[16] J. Park, D. M. Kim, E. D. Carvalho, and C. N. Manchón, "Hybrid precoding for massive MIMO systems in cloud RAN architecture with capacity-limited fronthauls," 2017, https://arxiv.org/abs/1709.07963.

[17] S. Payami, M. Ghoraishi, and M. Dianati, "Hybrid Beamforming for Large Antenna Arrays with Phase Shifter Selection," *IEEE Transactions on Wireless Communications*, 15, 2016, 7258–71.

[18] S. Payami, M. Ghoraishi, M. Dianati, and M. Sellathurai, "Hybrid Beamforming with a Reduced Number of Phase Shifters for Massive MIMO Systems," *IEEE Transactions on Vehicular Technology*, 67, 2018, 4843–51.

[19] S. Payami, N. Mysore Balasubramanya, C. Masouros, and M. Sellathurai, "Phase Shifters versus Switches: An Energy Efficiency Perspective on Hybrid Beamforming," *IEEE Wireless Communications Letters*, 8, 2019, 13–6.

[20] H. Ren, N. Liu, C. Pan, M. Elkashlan, A. Nallanathan, X. You, and L. Hanzo, "Low-latency C-RAN: An Next-generation Wireless Approach," *IEEE Transactions on Vehicular Technology*, 13, 2018, 48–56.

[21] Y. Shi, J. Zhang, and K. Letaief, "Group Sparse Beamforming for Green Cloud-RAN," *IEEE Transactions on Wireless Communications*, 13, 2014, 2809–23.

[22] S. Sun *et al.*, "Propagation Path Loss Models for 5G Urban Micro- and Macro-cellular Scenarios," in *Proceedings of IEEE 83rd Vehicular Technology Conference (VTC Spring)*, Nanjing, 2016.

[23] V. Suryaprakash, P. Rost, and G. Fettweis, "Are Heterogeneous Cloud-based Radio Access Networks Cost Effective?" *IEEE Journal on Selected Areas in Communications*, 33, 2015, 2239–51.

[24] S.-H. Tsai, "Equal Gain Transmission with Antenna Selection in MIMO Communications," *IEEE Transactions on Wireless Communications*, 10, 2011, 1470–9.

[25] T. Vu, D. Ngo, M. Dao, S. Durrani, D. Nguyen, and R. Middleton, "Energy Efficiency Maximization for Downlink Cloud Radio Access Networks with Data Sharing and Data Compression," *IEEE Transactions on Wireless Communications*, 17, 2018, 4955–70.

[26] D. Wang, Y. Wang, R. Sun, and X. Zhang, "Robust C-RAN Precoder Design for Wireless Fronthaul with Imperfect Channel State Information," in *IEEE Wireless Communications and Networking Conference (WCNC)*, San Francisco, 2017.

[27] A. Wiesel, Y. Eldar, and S. Shamai, "Linear Precoding via Conic Optimization for Fixed MIMO Receivers," *IEEE Transactions on Signal Processing*, 54, 2006, 161–76.

[28] Wireless InSite Propagation Software, https://www.remcom.com/wireless-insite-em-propagation-software.

[29] G. Xu, C.-H. Lin, W. Ma, S. Chen, and C.-Y. Chi, "Outage Constrained Robust Hybrid Coordinated Beamforming for Massive MIMO Enabled Heterogeneous Cellular Networks," *IEEE Access*, 5, 2017, 13601–16.

[30] A. Younis, T. Tran, and D. Pompili, "Energy Efficient Resource Allocation in C-RANs with Capacity-limited Fronthaul," *IEEE Transactions on Mobile Computing*, 20, 2021, 473–87.

[31] D. Zeng, J. Zhang, L. Gu, S. Guo, and J. Luo, "Energy-Efficient Coordinated Multipoint Scheduling in Green Cloud Radio Access Network," *IEEE Transactions on Vehicular Technology*, 67, 2018, 9922–30.